



UvA-DARE (Digital Academic Repository)

Seizure activity and brain damage in a model of focal non-convulsive status epilepticus

Vila Verde, D.; Zimmer, T.; Cattalini, A.; Pereira, M.F.; van Vliet, E.A.; Testa, G.; Gnatkovsky, V.; Aronica, E.; de Curtis, M.

DOI

[10.1111/nan.12693](https://doi.org/10.1111/nan.12693)

Publication date

2021

Document Version

Final published version

Published in

Neuropathology and Applied Neurobiology

License

Article 25fa Dutch Copyright Act

[Link to publication](#)

Citation for published version (APA):

Vila Verde, D., Zimmer, T., Cattalini, A., Pereira, M. F., van Vliet, E. A., Testa, G., Gnatkovsky, V., Aronica, E., & de Curtis, M. (2021). Seizure activity and brain damage in a model of focal non-convulsive *status epilepticus*. *Neuropathology and Applied Neurobiology*, 47(5), 679-693. <https://doi.org/10.1111/nan.12693>

General rights


It is not permitted to download or to forward/distribute the text or part of it without the consent of the author(s) and/or copyright holder(s), other than for strictly personal, individual use, unless the work is under an open content license (like Creative Commons).

Disclaimer/Complaints regulations

If you believe that digital publication of certain material infringes any of your rights or (privacy) interests, please let the Library know, stating your reasons. In case of a legitimate complaint, the Library will make the material inaccessible and/or remove it from the website. Please Ask the Library: <https://uba.uva.nl/en/contact>, or a letter to: Library of the University of Amsterdam, Secretariat, Singel 425, 1012 WP Amsterdam, The Netherlands. You will be contacted as soon as possible.

UvA-DARE is a service provided by the library of the University of Amsterdam (<https://dare.uva.nl>)

Seizure activity and brain damage in a model of focal non-convulsive *status epilepticus*

Diogo Vila Verde¹  | Till Zimmer² | Alessandro Cattalini¹ | Marlene F. Pereira^{3,4}  |
Erwin A. van Vliet^{2,5}  | Giuseppe Testa^{3,4} | Vadym Gnatkovsky¹ | Eleonora Aronica^{2,6} |
Marco de Curtis¹ 

¹Epilepsy Unit, Fondazione Istituto Neurologico Carlo Besta, Milan, Italy

²Department of (Neuro) Pathology, Amsterdam UMC, University of Amsterdam, Amsterdam Neuroscience, Amsterdam, The Netherlands

³Department of Oncology and Hematooncology, University of Milan, Milan, Italy

⁴Laboratory of Stem Cell Epigenetics, IEO, European Institute of Oncology, IRCCS, Milan, Italy

⁵Swammerdam Institute for Life Sciences, Center for Neuroscience, University of Amsterdam, Amsterdam, The Netherlands

⁶Stichting Epilepsie Instellingen Nederland (SEIN), Heemstede, The Netherlands

Correspondence

Marco de Curtis, Epilepsy Unit, Fondazione Istituto Neurologico Carlo Besta, via Celoria 11, Milan, Italy.
Email: marco.decurtis@istituto-besta.it

Funding information

Italian Health Ministry; Associazione Paolo Zorzi pe le Neuroscienze; H2020 Marie Skłodowska-Curie Actions, Grant/Award Number: 722053 and 765966

Abstract

Aims: Focal non-convulsive *status epilepticus* (FncSE) is a common emergency condition that may present as the first epileptic manifestation. In recent years, it has become increasingly clear that *de novo* FncSE should be promptly treated to improve post-status outcome. Whether seizure activity occurring during the course of the FncSE contributes to ensuing brain damage has not been demonstrated unequivocally and is here addressed.

Methods: We used continuous video-EEG monitoring to characterise an acute experimental FncSE model induced by unilateral intrahippocampal injection of kainic acid (KA) in guinea pigs. Immunohistochemistry and mRNA expression analysis were utilised to detect and quantify brain injury, 3-days and 1-month after FncSE.

Results: Seizure activity occurring during the course of FncSE involved both hippocampi equally. Neuronal loss, blood-brain barrier permeability changes, gliosis and up-regulation of inflammation, activity-induced and astrocyte-specific genes were observed in the KA-injected hippocampus. Diazepam treatment reduced FncSE duration and KA-induced neuropathological damage. In the contralateral hippocampus, transient and possibly reversible gliosis with increase of aquaporin-4 and Kir4.1 genes were observed 3 days post-KA. No tissue injury and gene expression changes were found 1-month after FncSE.

Conclusions: In our model, focal seizures occurring during FncSE worsen ipsilateral KA-induced tissue damage. FncSE only transiently activated glia in regions remote from KA-injection, suggesting that seizure activity during FncSE without local pathogenic co-factors does not promote long-lasting detrimental changes in the brain. These findings demonstrate that in our experimental model, brain damage remains circumscribed to the area where the primary cause (KA) of the FncSE acts. Our study emphasises the need to use antiepileptic drugs to contain local damage induced by focal seizures that occur during FncSE.

KEYWORDS

seizures, brain damage, non-convulsive status epilepticus, epilepsy, hippocampus

INTRODUCTION

One of the recurrent questions in epilepsy research is whether seizures during *status epilepticus* (SE) can cause brain damage. While there is increasing experimental evidence that generalised convulsive SE produces long-lasting neuropathological changes in the brain of rodents and humans [1, 2], it has been questioned whether seizure events that commonly occur during focal non-convulsive *status epilepticus* (FncSE) results in long-term consequences and contributes to pathology [3]. The need to recognise if seizure activity during FncSE aggravates brain damage is critical, even more since seizures during FncSE are often overlooked and consequently not properly treated [4].

Human studies and clinical data have proven controversial, since it is not easy to distinguish seizure-induced brain damage from the underlying cause that triggers FncSE [5]. While one study has demonstrated that seizures during FncSE without an evident acute brain injury can trigger the production of blood biomarkers of neuronal damage [6], others have found that patients suffering from FncSE do not develop long-term cognitive, memory or behavioural deficits [7–10]. Also, animal data have not proven conclusive, since brain damage has been mainly evaluated in models that do not accurately represent a proper FncSE condition. Intraperitoneal injection with either pilocarpine or kainic acid (KA) induces an acute convulsive SE and widespread multifocal damage [11–13], and for these reasons cannot be considered pure models of focal SE [14]. Intracerebral KA injection offers a better approach to study focal ictogenesis and epileptogenesis [15]. Intra-hippocampal [16–19], intra-amygdala [20–22] or intracortical [23] microinjections of KA result in pathological alterations resembling hippocampal sclerosis. Some of these studies proposed that the acute SE promotes secondary epileptogenesis and alterations in brain regions remote to the KA injection site [17, 20, 21, 24, 25]. Nevertheless, intracerebral KA injection may promote either FncSE or secondarily convulsive SE, depending on the protocol (dose, site of injection, etc.) and animal species [16, 18–20, 26]. Moreover focal electrical stimulation of the perforant path or other limbic structures can also induce either focal or secondary convulsive SE, with or without damage beyond the area of stimulation [27–31]. In conclusion, the aforementioned experimental models do not unequivocally resolve whether focal seizures occurring during FncSE have an impact on the extent, severity or distribution of brain damage.

Here, we investigated how much acute seizure activity *per se* affects the development of both localised and remote brain damage in a model of FncSE, defined as a model in which focal seizures predominantly occur during the acute SE [5]. The present report extends preliminary observations [32] by focusing on RNA expression changes and glial activation patterns that transiently occur outside the KA-injected region.

MATERIAL AND METHODS

The study is based on a population of 49 adult female Hartley guinea pigs (250–300 g, 3 postnatal weeks of age; Charles River, Calco,

Italy), housed in a 12-h light-dark controlled cycle environment with *ad libitum* food and water supply. The experimental protocol was reviewed and approved by the Animal Welfare Office of the Italian Health Ministry (Authorization n. 36/2016-PR), in accordance with the European Committee Council Directive (2010/63/EU) and with the 3Rs principle. Efforts were made to minimise the number of animals and their suffering. Thirty-four animals were processed for molecular analysis and 15 were submitted to gene expression analysis (see below).

Electrode implantation and unilateral intrahippocampal injection

Forty-four guinea pigs were surgically implanted with bilateral intrahippocampal (AP –3 mm, ML ±3 mm, DV –3.25 mm relatively to Bregma) and epidural EEG recording electrodes, as described previously [33]. Seven days after electrode implantation, animals were injected in the dorsal *cornu ammonis* (CA1) of the right hippocampus with either a solution containing kainic acid (KA; $n = 34$) or 0.9% NaCl saline (sham operated animals; $n = 10$) under continuous video-EEG recording. A 30-gauge needle, connected to a 5 μ l Hamilton syringe, was lowered through the guide cannula in the right hippocampus to inject a volume of 1 μ l 0.9% NaCl solution with 1 μ g KA (Sigma, St. Louis, MO, USA) over a period of 2 min. The needle was kept in place for 2 min to prevent backflow of the injected solution. Within 10 min after KA injection, epileptiform activity typical of a focal non-convulsive *status epilepticus* (FncSE) was recorded in all animals. Six animals were twice injected *i.p.* with diazepam (DZP; 25 μ l/kg dissolved in NaCl) 30 min before and 30 min after KA injection (12.5 μ l/kg). Sham animals were injected in the right hippocampus with 1 μ l 0.9% NaCl following the same procedure. None of the sham operated/injected guinea pigs showed epileptiform activity. Acute animals were recorded for 3 days post-KA injection; chronic animals were video-EEG recorded for no less than 4 weeks after FncSE, to verify the presence of spontaneous seizures [33, 34]. Video-EEG monitoring was performed in 10 sham-operated/treated animals, 28 KA-injected guinea pigs and in 6 KA-injected animals treated with DZP (DZP+KA). A fifth group of naïve animals was used but not video-EEG monitored ($n = 5$).

Video-EEG recordings

Continuous 24/24-hour video-EEG monitoring started 1 week after surgery; implanted pedestals were connected to a cable mounted on a swivel coupled to the preamplifier of a BrainQuick EEG System (Micromed, Mogliano Veneto, Italy). Synchronised video-EEG was continuously recorded 48 h before injection, during the induction of FncSE and for the following 3 days in the acute animals (KA and DZP+KA) and for 4 weeks in the chronic KA group. EEG data were recorded at 0.1–1.0 kHz, 2064 Hz sampling rate, with 16-bit precision and high-pass filter at 0.1 Hz,

using the System Plus Evolution (Micromed). Video signals were simultaneously acquired with digital cameras to detect motor events. Video-EEG was analysed offline and hippocampal EEG patterns were identified and quantified for each animal. The EEG activity recorded with epidural electrodes was used to identify diffuse seizure patterns. KA-induced epileptiform activity was characterised by seizures combined with continuous 1–3 Hz spiking [32–34]. Seizure events during KA-induced FncSE were defined by researchers that were blinded to the treatment group. Seizures were also automatically counted with a software developed by Vadym Gnatkovsky to analyse long EEG recording periods with a compressed time scale. Seizure discharges were identified as focal unilateral, bilateral, convulsive or non-convulsive based on the EEG pattern distribution and on video analysis. In the chronic animals, spontaneous focal seizures were identified with 24/24-hour video-EEG monitoring recorded every other week for 4 weeks; the features of chronic spontaneous seizures were comparable to those described in previous studies [33, 34]. In these animals, FncSE profile was similar to the animals sacrificed at 3 days.

Immunohistochemical analysis

Following video-EEG recordings, animals were anaesthetised with sodium thiopental (125 mg/kg i.p., Farmotal; Pharmacia, Milan, Italy) and were trans-cardially perfused with 0.9% NaCl, followed by 4% paraformaldehyde in phosphate buffer 0.1 M for 5 min. Brains were explanted, immersed in 4% paraformaldehyde for 24 h and cut into 50 μ m coronal sections. For immunohistochemical processing, the following antibodies were used: (a) monoclonal mouse anti-neuronal nuclei (NeuN 1:1000 – Merck-Millipore, Darmstadt, Germany); (b) mouse anti-microtubule associated protein 2 (MAP2 1:1000 – Neomarker-Invitrogen, Fremont, CA, USA); (c) polyclonal rabbit anti-glial fibrillary acid protein (GFAP 1:500 – DAKO, Glostrup, Denmark); (d) ionised calcium-binding adapter molecule 1 (Iba-1 1:200 – Merck-Millipore, Darmstadt, Germany) and (e) Immunoglobulin G (IgG 1:200 – Vector Laboratories, Burlingame, CA USA). Two serial coronal sections *per animal* were selected and analysed by researchers that were blinded to the treatment group. A standardised protocol was used for histochemical staining [32,33]. Immuno-stained sections were digitised using Scanscope software (Aperio Technologies, Sausalito, CA, USA). Staining for NeuN, MAP2, GFAP and IgG were analysed in naïve, sham-treated, acute KA, acute DZP+KA and chronic KA animals. Quantitative field fraction estimates of these immunostains were carried out in both hippocampi using Image-Pro Plus 7 software (Media Cybernetics, Inc. Rockville, MD, USA). Specific immunostaining density was estimated at 5x magnification in 2 regions of interest (ROIs) positioned in CA1, CA3 and dentate gyrus (DG) with respect to background signal. For each ROI densitometry was automatically calculated by the software on 2 adjacent slices in each hippocampal subfield (18 ROIs *per brain slice*; 3 ROIs *per subfield*) ipsilateral (right) and contralateral (left)

to KA injection. Densitometric ROIs were positioned at least 0.5 mm away from the electrode tracks. For three dimensional reconstruction of microglial cells, immunofluorescence for Iba-1 and DAPI (1:5000) conjugated to Cy3 was performed on 50 μ m thick coronal sections.

Fluoro-jade staining

Sections were mounted and then treated with 0.06% potassium permanganate for 15 min, washed 3 times, immersed in 0.001% FJ (Histo-Chem, Inc., Jefferson, Arkansas, USA) in 0.1% acetic acid for 30 min and rinsed in distilled water. After drying, slides were clarified in xylene and cover slipped with distyrene plasticizer xylene (DPX; BDH Lab Supplies, Leicestershire, UK) [32]. All fluoro-jade positive (FJ⁺) cells were counted using FIJI-ImageJ (v2.0.0). Non-overlapping fields in CA1, CA3 and DG areas of both ipsi- and contralateral hippocampi were captured under identical conditions at 20x and 40x magnification with a Leica TCS SP8 microscope (Leica Microsystems, Germany). Cell counting was independently performed by 2 investigators in each experimental group (2 sections *per animal*, 0.5 mm away from the electrode tracks).

Morphometric analysis of microglia

Sections were visualised using a Leica SP8 confocal microscope (Leica Microsystems, Germany), applying the LASX software with navigator (version 3.1.5.16). Regions in dorsal CA1 *stratum radiatum* and the *hilus* of DG were acquired at high resolution (2 sections *per animal*, 0.5 mm away from the electrode tracks) using a 63X/1.4 oil objective with a x-y sampling of 72 nm. Cells were eligible for reconstruction if the following criteria were met: i) an Iba-1 positive cell was surrounding a single DAPI-stained nucleus; ii) the cell did not have truncated processes; iii) the cell was sufficiently separated from neighbouring cells to ensure correct reconstruction. A total of 240 cells, 120 for CA1 and 120 for DG, were selected for reconstruction performed using simple neurite tracer available in FIJI-ImageJ software (v2.0.0) [35]. Microglial morphometric properties were evaluated by quantifying the number of processes, total length, average number of intersections and Sholl analysis (number of intersections at radial intervals of 2 μ m starting from the soma central point).

RNA isolation and quantitative real-time PCR measurements

Fresh hippocampal brain tissue for gene expression analysis was obtained from a group of 5 sham-operated and KA-injected guinea pigs either 3 days ($n = 5$) or 4 weeks ($n = 5$) post-injection. After saline intra-cardiac perfusion, brains were removed and the

whole hippocampus dissected out on a cold Petri dish. Dorsal CA1 and DG ipsilateral and contralateral to KA injection were further dissected and separately stored at -80°C . Samples were shipped to Amsterdam UMC where gene expression analysis was performed. Frozen brain tissue was homogenised in 700 μL Qiazol Lysis Reagent (Qiagen Benelux, Venlo, the Netherlands). Total RNA was isolated using the miRNeasy Mini kit (Qiagen Benelux, Venlo, the Netherlands) according to the manufacturer's instructions. RNA concentration and purity were determined at 260/280 nm using a Nanodrop 2000 spectrophotometer (Thermo Fisher Scientific, Waltham, MA, USA). To evaluate mRNA expression, 1 μg tissue-derived total RNA was reverse-transcribed into cDNA using oligo-dT primers. PCRs were run on a thermocycler (Lightcycler 480, Roche Applied Science, Basel, Switzerland) using housekeeping reference genes actin and glyceraldehyde 3-phosphate dehydrogenase (GAPDH). PCR mix contained 1 μL cDNA, 2.5 μL SensiFAST SYBR Green NoROX kit (Bioline Reagents Limited, London, UK), 0.4 μM of forward/reverse primers plus water to a final volume of 5 μL /well. PCR reactions were run in duplicates and a negative control containing water instead of cDNA was included for each gene in each run. Cycling conditions were as follows: initial denaturation at 95°C for 5 min, followed by 45 cycles of denaturation at 95°C for 15 s, annealing at 65°C for 5 s and extension at 72°C for 10 s. Sample fluorescence was measured via single acquisition mode at 72°C after each cycle. Primer specificity was assessed using melt curve analysis after each run. To analyse potentially relevant pathogenic elements (inflammation, glial function, activity-dependent changes) associated with brain damage, the following genes were analysed: (a) interleukin 1 beta (IL-1 β); (b) cyclo-oxygenase-2 (COX-2); (c) haem oxygenase 1 (HO-1); (d) c-FOS; (e) aquaporin-4 (AQP4) and (f) inwardly rectifying potassium channel 4.1 (Kir4.1). Quantification of data was performed using LinRegPCR as described elsewhere [36].

Statistical analysis

Statistical analysis was performed using Prism 8.2 (GraphPad Software Inc., San Francisco, CA, USA). After identification of outliers (ROUT method), the Shapiro–Wilk normality test was performed to assess normality of the distribution. Where a normal distribution was found, one-way analysis of variance (ANOVA) was used to compare four independent groups and a paired or unpaired Student *t*-test to match 2 groups directly, for dependent or independent data respectively. When the data was not normally distributed, the non-parametric Kruskal–Wallis test followed by a Mann–Whitney *U* post-hoc test was employed to compare four independent groups and a paired Wilcoxon signed-rank test to relate two groups against each other. In the morphology data, results are expressed as means \pm standard deviation (SD) for the number of independent experiments (*n*). The remaining graphical data is illustrated with boxplots with min., max., median and quartiles shown. The confidence interval

($1-\alpha$) was set as 95% (0.95) so that the difference between means was considered statistically significant at *p* values of less than 5% (0.05), 1% (0.01), 0.1% (0.001) and 0.01% (0.0001) of significance level (α).

RESULTS

Focal non-convulsive *status epilepticus* (FncSE) was induced in 34 guinea pigs. Of these, 14 were sacrificed 3 days post-KA injection (acute post-FncSE phase) to evaluate the peak phase of brain damage [32, 34]. A different group of animals (*n* = 14; KA chronic group) was sacrificed 4 weeks post-KA injection [33, 34]. We treated another group of animals with intraperitoneal diazepam (DZP) before KA injection (DZP+KA group; *n* = 6). Sham-operated animals (*n* = 10) were injected in one hippocampus with saline solution. Video-EEG, immunohistochemical and morphological evaluations were performed in a total of 5 naïve, 5 sham, 9 acute post-KA, 9 KA chronic and 6 DZP+KA animals. Gene expression analysis was performed in 5 sham, 5 acute post-KA and 5 KA chronic guinea pigs.

Within 10 min of KA injection, FncSE started in the injected right hippocampus (ipsilateral KA in Figure 1A) and subsequently propagated within 1 min to the contralateral hippocampus. Seizures occurring during FncSE were classified by video-EEG monitoring as non-convulsive or secondarily convulsive according to the Racine scale [37] (stages 1–3 correspond to non-convulsive phenotype and 4/5 to convulsive phenotype with bilateral and diffuse EEG discharges). In the KA groups, seizures during FncSE were $89.1 \pm 12.9\%$ non-convulsive (Figure 1G), with the most common phenotype observed being mouth and head myoclonus with the occasional unilateral front limb myoclonus [34]. A total of 115 focal secondarily convulsive seizures lasting less than 30 s were counted among 1071 seizures occurring during the FncSE in all 18 animals. The time spent in secondarily convulsive seizures was minimal compared to the duration of the SE. In only 4 animals 10 to 15 convulsive seizures were observed (out of 353; Figure 1F), while the remaining 14 animals had from 1 to 3 convulsions (Figure 1F). The inclusion of the four animals with >10 convulsive seizures did not modify the overall immunostaining densitometric results (see below). None of the animals processed for the RNA expression analysis showed convulsive seizures during FncSE. The large majority of focal seizures recorded during the FncSE ($79.7 \pm 11.9\%$) involved both the KA injected and the contralateral hippocampi (Figure 1H) with no cortical EEG involvement. Epileptiform activity was not detected in sham animals recorded for 6 h after intrahippocampal saline injection (data not shown). As illustrated in Figure 1B, C and E, FncSE duration was 8.3 ± 2.0 h in KA-injected animals (*n* = 18) and was significantly shorter in the DZP+KA group (3.5 ± 1.5 h; *n* = 6). Moreover the number of seizures *per* animal was higher in the KA group (63.5 ± 14.3 seizures *per* animal; *n* = 18) in comparison to the DZP+KA group (11 ± 6.3 seizures *per* animal; *n* = 6; Figure 1D).

Animals were sacrificed and brains were processed for morphological analysis either 3 days or 4 weeks post FncSE. First, we

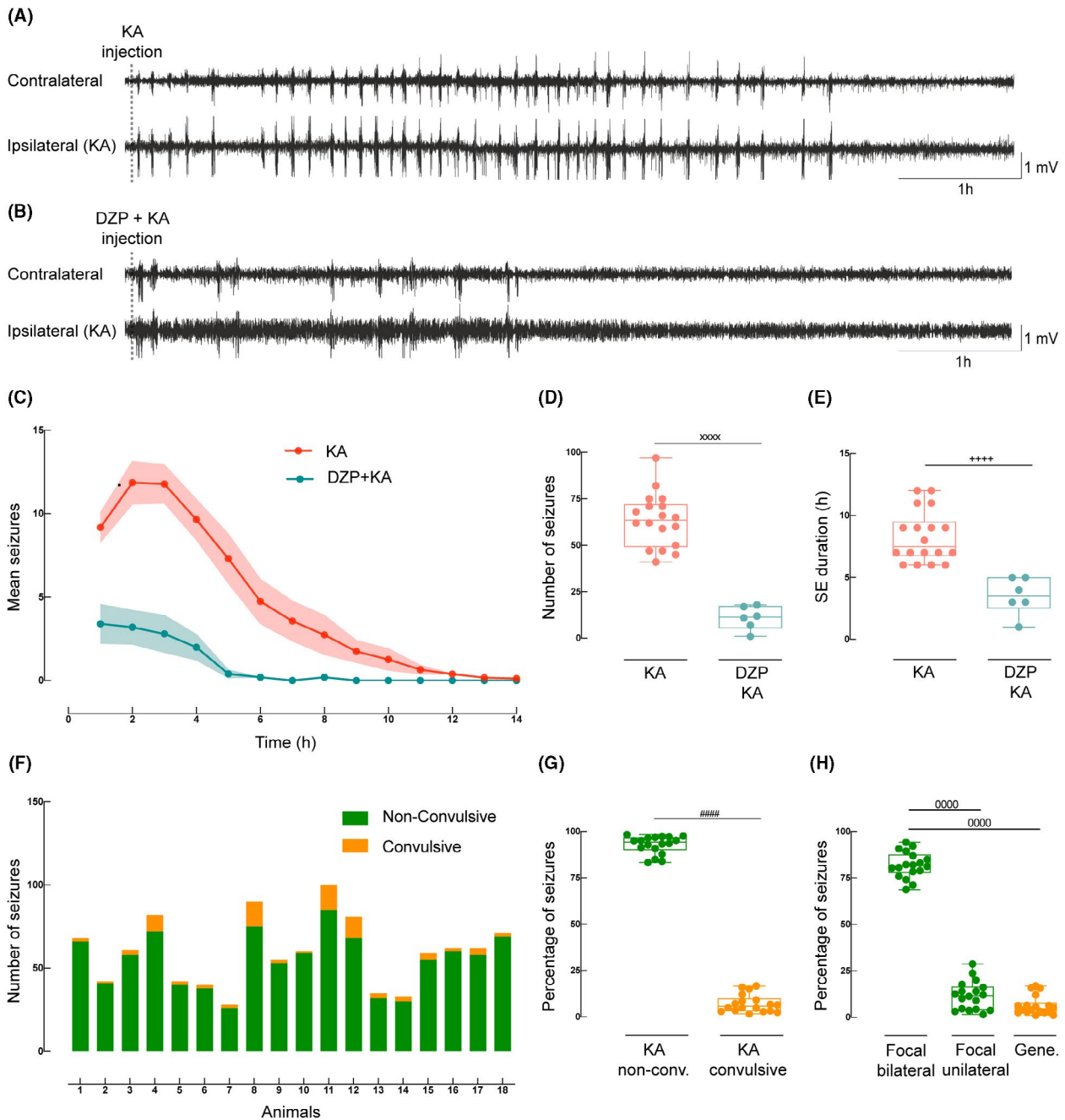


FIGURE 1 EEG and seizure features during the focal non convulsive *status epilepticus* induced by unilateral intrahippocampal KA injection in KA and diazepam +KA animals. EEG analysis was performed in 18 KA animals (9 processed 3 days after SE onset, and 9 chronic KA animals recorded/analysed in acute phase - $n = 18$) and in 6 DZP+KA animals ($n = 6$). (A) Compressed 7 h EEG recording from left (contralateral) and right [ipsilateral (KA)] hippocampus after KA injection in the dorsal CA1 area of right hippocampus (vertical dotted line on both traces). (B) Compressed 7 h EEG recording from left (contralateral) and right [ipsilateral (KA)] hippocampus after intraperitoneal administration of diazepam (DZP) followed by intrahippocampal KA injection. (C) Mean seizures *per hour* after KA injection (red trace) and KA preceded by DZP (blue trace). (D) Number of seizures *per animal* treated with KA injection (red) vs DZP+KA (blue). (xxxx): $p < 0.0001$ (unpaired t-test). (E) *Status epilepticus* duration in hours *per animal* after KA injection (red) vs DZP+KA (blue). ($^{++++}$): $p < 0.0001$ (Mann-Whitney U test). (F) Number of convulsive (yellow) and non-convulsive (green) seizures for each animal individually. (G) Percentage of seizures characterised by a convulsive (yellow) vs non-convulsive phenotype (green); one dot *per column* represents the same animal. ($^{####}$): $p < 0.0001$ (Wilcoxon signed-rank test). (H) Percentage of seizures *per animal* defined as focal bilateral (green) vs focal unilateral (green) vs generalised (yellow). (0000): $p < 0.0001$ (paired t-test)

assessed two weeks after implantation if the surgery procedure provoked any type of damage with densitometric analysis of NeuN, MAP2, GFAP and IgG in CA1, CA3 and DG of naïve animals ($n = 5$) vs

sham-operated animals ($n = 5$). No statistical difference was found by comparing these two groups (Figure S1A–D); therefore, the sham group was used as our control condition throughout the study.

Densitometric measurements separately performed in the hippocampus ipsilateral (KA+seizures) and contralateral (seizures only) to the KA-injection were compared to their respective regions in sham-operated animals and DZP+KA (Figures 2B–C and 4B–C). As

previously shown in a different group of animals [32], the densitometric values of NeuN and MAP2, 3 days post-KA, in the ipsilateral CA1, CA3 and DG (only NeuN) were lower with respect to the homologous subfields of sham-operated animals (Figure 2B–C, representative

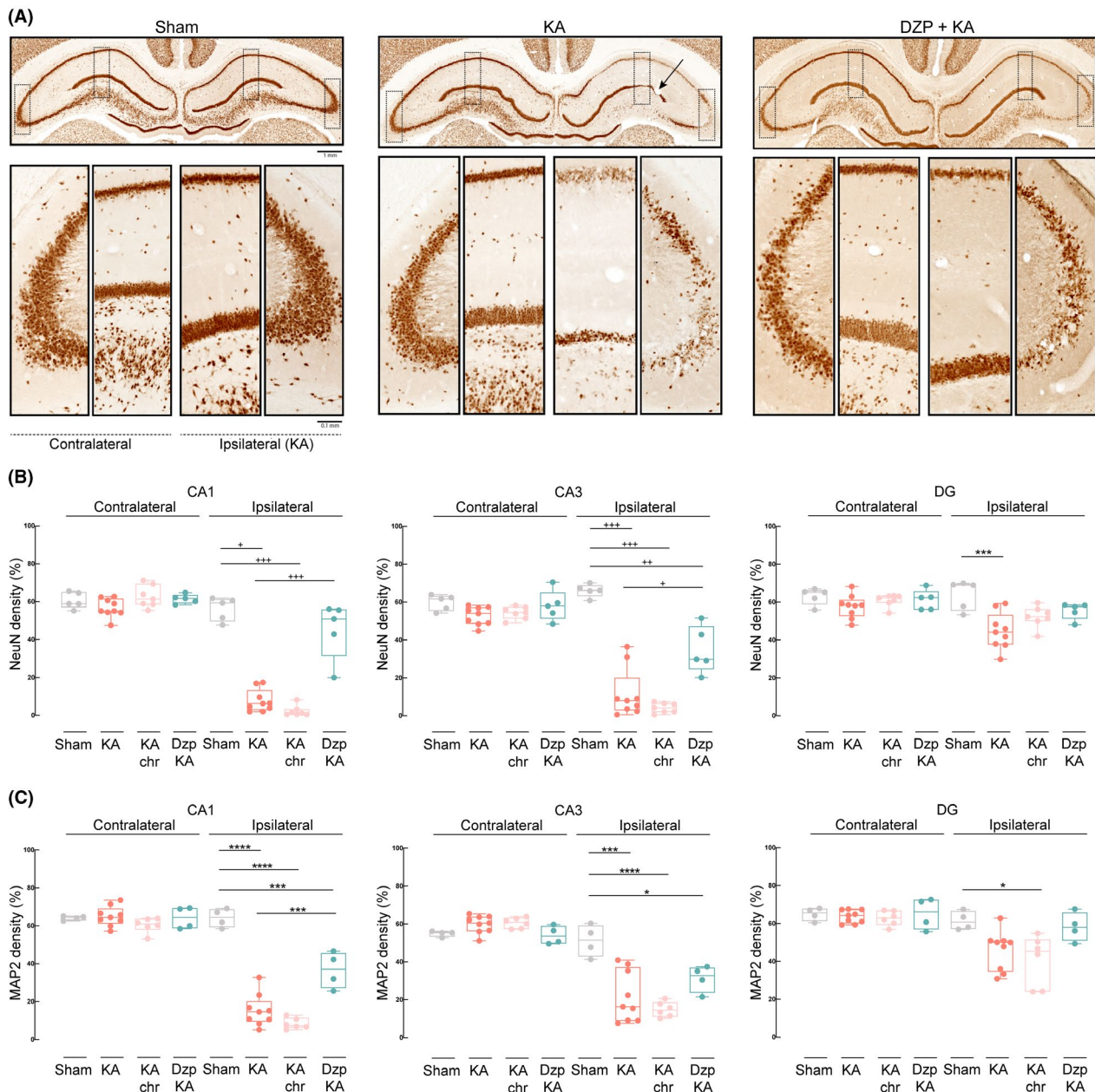


FIGURE 2 NeuN and MAP2 semi-quantitative densitometry analysis. (A) NeuN immunostained coronal sections represented at low (upper pictures) and high magnification (lower pictures; dotted area outlined in the upper photographs) for sham (left), KA (middle) and DZP+KA (right) animals 3 days post-KA. KA was injected in the right dorsal CA1 region (injection cannula artifact marked by arrowhead in the middle panel). Left and right hemispheres contralateral and ipsilateral to hippocampal KA injection, respectively, are illustrated. Calibration bars in higher magnification =0.1 mm and in lower magnification =1 mm. For B and C: Grey plots: sham-operated animals. Red plots: 3 days post-KA injection (KA). Pink plots: 1 month post-KA injection animals (KA chronic). Green plots: animals treated with DZP and KA injected (DZP+KA). Average percentage of densitometric changes in the KA-injected (ipsilateral) and contralateral hippocampal CA1 (left panels), CA3 (middle panels) and DG (right panels) subregions are illustrated. (B) NeuN densitometric values obtained from sham ($n = 5$), KA ($n = 9$), KA chronic ($n = 7$) and DZP+KA ($n = 5$) guinea pigs. (*): $p < 0.05$; (**): $p < 0.01$; (***): $p < 0.001$ (Mann-Whitney U test); (****): $p < 0.0001$ [one-way analysis of variance (ANOVA)]. (C) MAP2 densitometric changes from the same areas of sham ($n = 4$), KA ($n = 9$), KA chronic ($n = 6$) and DZP+KA injection ($n = 4$) guinea pigs. (*): $p < 0.05$; (**): $p < 0.01$; (***): $p < 0.001$; (****): $p < 0.0001$ (ANOVA)

panels in Figure 2A). The neuronal loss in the KA-injected CA1, CA3 and DG observed in the acute phase remained in the KA chronic group, except for the DG when compared to the 3-days KA group (Figure 2B,C; Figure S1 E). Interestingly, densitometric NeuN and MAP2 values in the DZP+KA animal group (Figure 2B,C; also, right panel in Figure 2A) were higher than the 3 days KA group for all subfields and were similar to the sham-group for NeuN in CA1 and DG and for MAP2 in DG. Of note, in the DZP+KA groups the values in CA3 for NeuN and in CA1, CA3 for MAP2 were lower compared to the sham groups (Figure 2B,C). NeuN and MAP2 densitometric values did not differ in the contralateral hippocampi of both KA (at 3 days and 4 weeks) and DZP+KA animals when compared to their respective sham-controls (Figure 2B,C). In line with these findings, fluoro-jade positive cells (FJ⁺) in the ipsilateral CA1, CA3 and DG were observed exclusively and consistently in the 3 days post-KA

injection and DZP+KA groups (Figure 3B, also representative panel 3A). FJ⁺ cells were never detected either 4 weeks post-KA or the hippocampus contralateral to KA injection in any group (Figure 3B). NeuN, MAP2, GFAP and IgG staining patterns were identical when the four animals that featured >10 convulsive seizures were excluded from the densitometric analysis and also when data from those four animals were compared against the remaining five animals from the same group that experienced only focal seizures (Figure S2).

Next, we investigated astrocytic activation in the same animal groups. As illustrated in Figure 4A astrogliosis was induced by KA injection. The densitometric values were higher in all subfields ipsilateral to KA injection at 3 days post-FncSE when compared to the sham-group (Figure 4B; also, middle column in Figure 4A). High GFAP immuno-density was maintained in CA1 and DG of the KA chronic group (Figure 4B; also, right column in Figure S1E). DZP+KA

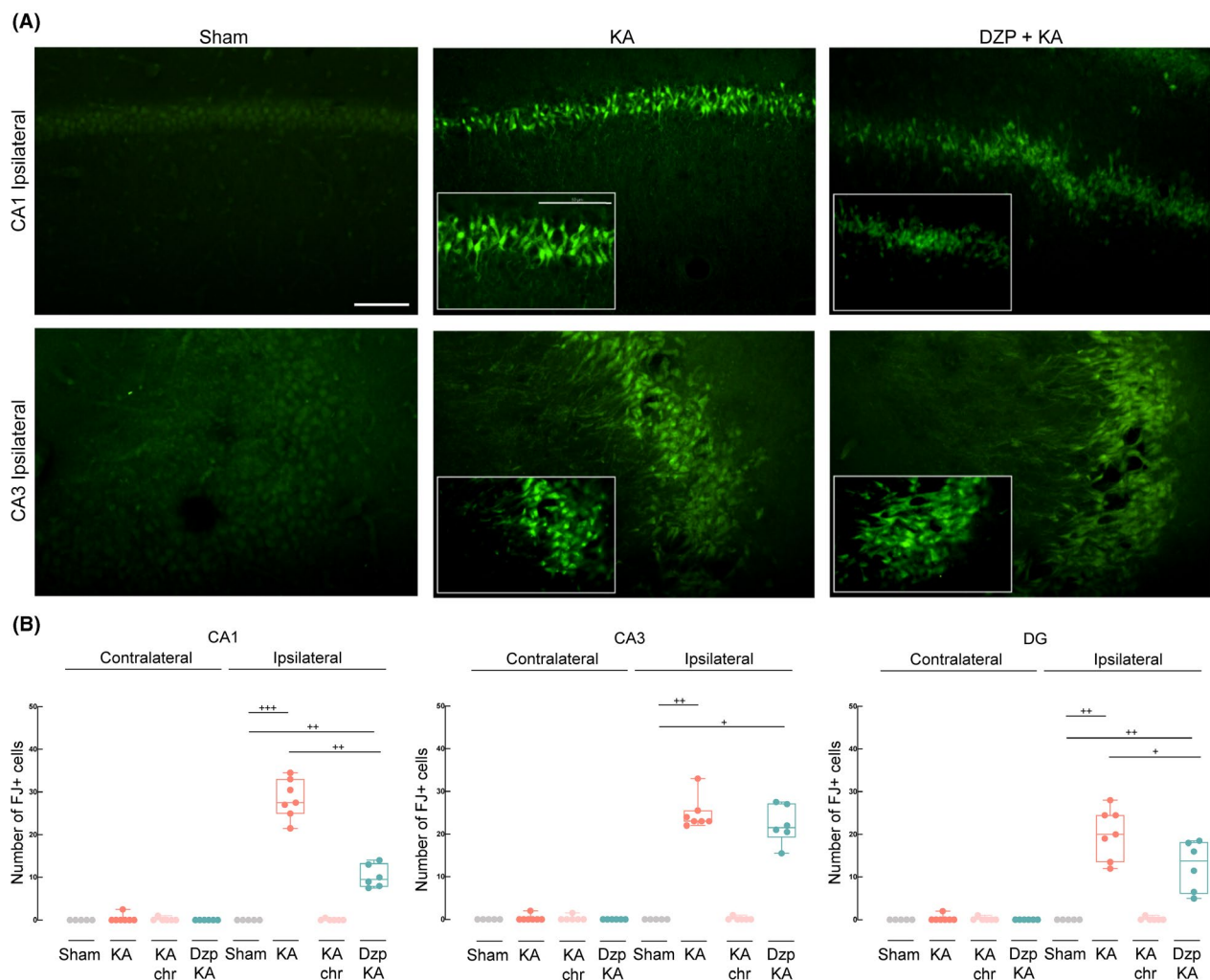


FIGURE 3 Fluoro-jade immunostaining and quantification in CA1, CA3 and DG subregions. (A) Representative micrographs of CA1 (upper part) and CA3 (lower part) subregions in the right hippocampi ipsilateral to the injection of sham-operated (left column), 3 day post-KA injection (middle column) and DZP+KA injection (right column) guinea pigs. Higher magnification photos are illustrated in the inserts. Calibration bars at higher magnification =50 μm and at lower magnification =100 μm. (B) Comparison between number of fluoro-jade⁺ cells in the KA injected (ipsilateral) and contralateral hippocampal subregions. In all graphics, grey, red, pink and green plots show counts from sham ($n = 5$), KA 3 days after FncSE ($n = 7$), chronic KA ($n = 6$) and DZP+KA ($n = 6$) guinea pigs, respectively. (*): $p < 0.05$; (**): $p < 0.01$; (**+): $p < 0.001$ (Mann-Whitney U test)

treated animals had the same high densitometric profile of the 3 days post-KA injected guinea pigs (Figure 4B, also right column in Figure 4A). Unlike previously noted [32], higher GFAP densitometry

values were also observed in the contralateral hippocampus of both KA (CA1, CA3 and DG; Figure 4B) and DZP+KA animals (CA3 and DG; Figure 4B) in comparison to sham-operated animals. Control

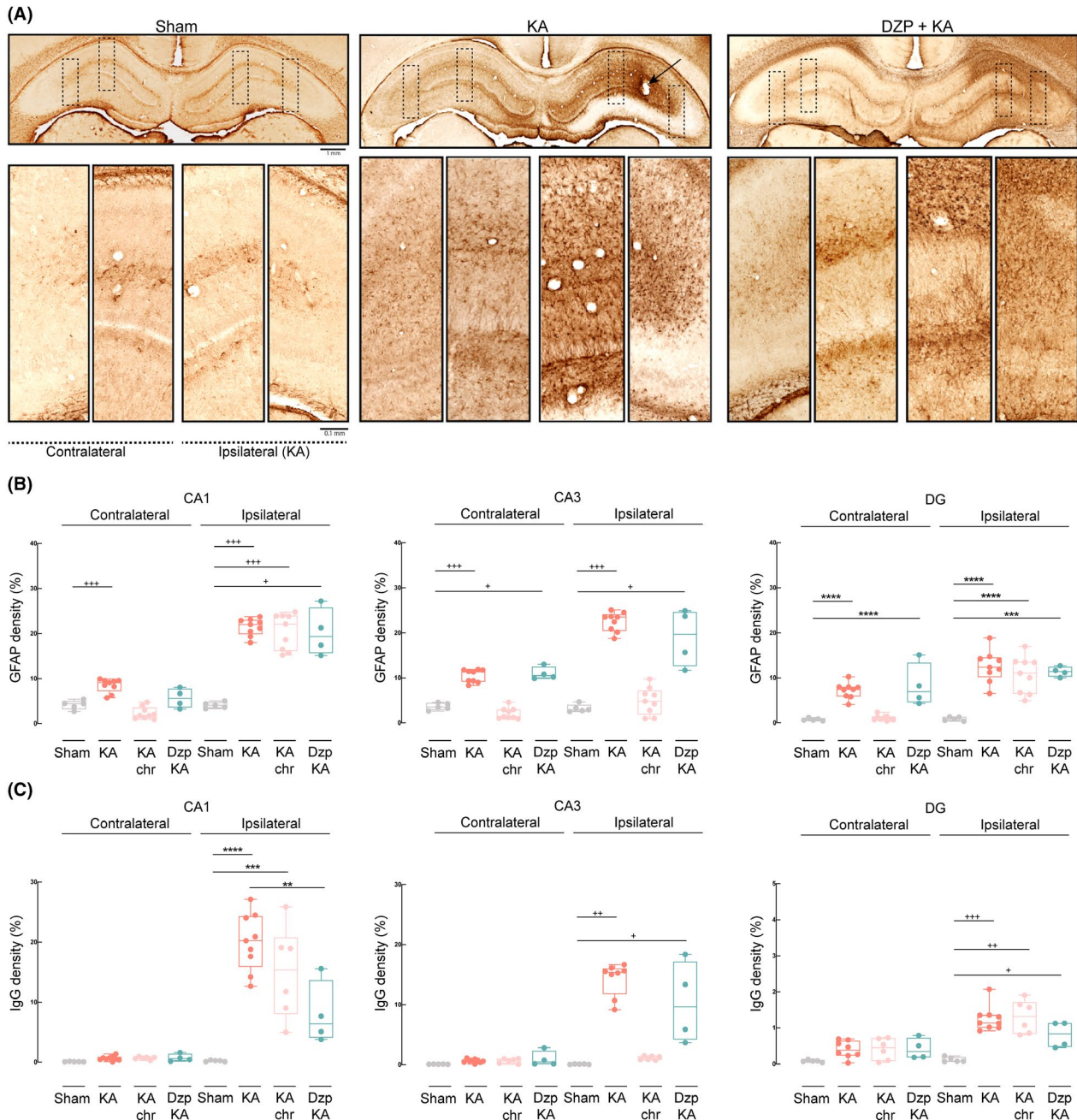


FIGURE 4 GFAP and IgG semi-quantitative densitometry analysis. (A) GFAP immunostained coronal sections are represented at low (upper pictures) and high magnification (lower pictures; dotted area outlined in the upper photographs) for sham (left panel), KA (middle panel) and DZP+KA (right panel) animals 3 days post-KA. Left and right hemispheres are marked as contralateral and ipsilateral (KA) respectively. Arrows mark in the upper middle panel points to the track of the intrahippocampal injection needle. Calibration bars in higher magnification = 0.1 mm and in lower magnification = 1 mm. (B and C): Average percentage of densitometric changes in the KA injected (ipsilateral) and contralateral hippocampal CA1, CA3 and DG subregions. Grey plots: sham-operated animals. Red plots: 3 days post-KA injection guinea pigs (KA). Pink plots: 1 month post-KA injection animals (KA chronic). Green plots: animals treated with DZP and KA injected (DZP+KA). (B) GFAP densitometric changes from sham ($n = 5$), KA ($n = 9$), KA chronic ($n = 9$) and DZP+KA ($n = 4$) guinea pigs. (*): $p < 0.05$; (**): $p < 0.01$; (***) $p < 0.001$ (Mann-Whitney U test); (****): $p < 0.0001$ (ANOVA). (C) Average percentage of densitometric IgG staining in sham ($n = 5$), KA ($n = 9$), KA chronic ($n = 6$) and DZP+KA ($n = 4$) guinea pigs. (*): $p < 0.05$; (**): $p < 0.01$; (***) $p < 0.001$ (Mann-Whitney U test); (****): $p < 0.0001$ (ANOVA)

values were observed in contralateral hippocampi 4 weeks after KA (Figure 4B; see also right panel in Figure S1E).

Finally, we observed higher IgG densitometry values in the ipsilateral hippocampus 3 days post-KA injection in all regions compared to the sham group (Figure 4C); these values were similar in CA1 and DG 4 weeks post-KA injection (Figure 4C). Furthermore, in the CA1 and DG 4 weeks post-KA injection (Figure 4C). Furthermore, in the DZP+KA group, CA3 and DG values were higher than the sham guinea pigs (Figure 4C). IgG staining was never observed in the contralateral hippocampus (Figure 4C). Overall, these data suggest that

KA induced a local increase in BBB permeability [38] exclusively in the KA-injected hippocampus.

To further evaluate glial involvement in KA-induced FncSE, we also investigated with Iba-1 immunofluorescence, the morphological changes of microglia cells in the hippocampi ipsilateral and contralateral to KA injection (Figure 5A and F). Sholl analysis employed to quantify the number of intersections at radial intervals of 2 μm starting from the soma (Figure 5B–E) showed smaller values in the ipsi- (CA1 and DG) and contralateral (CA1) hippocampi of KA

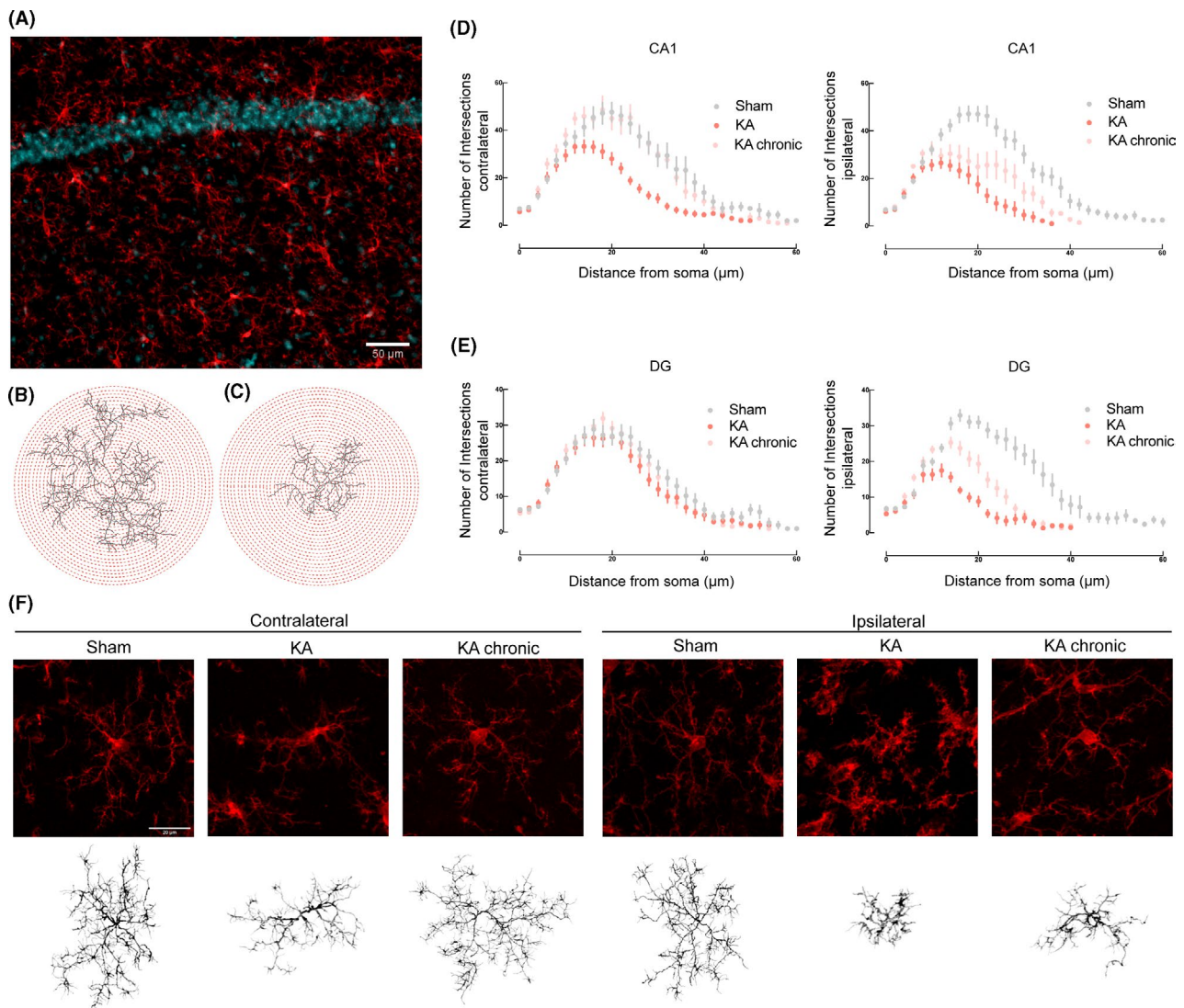


FIGURE 5 Morphological analysis and reconstruction of microglial cells in hippocampal CA1 and DG. (A) Representative immunofluorescence of a hippocampal coronal section of CA1 pyramidal layer: neurons marked by DAPI in blue, microglia stained by Iba-1 in red. Calibration bar = 50 μm . (B) Representative Sholl analysis setting of a manually reconstructed microglia cell from a KA animal (contralateral hippocampus) and (C) from the ipsilateral hippocampus of the same animal. The circles centred around the soma are separated by radial intervals of 2 μm . (D) Number of intersections *per* 2 μm radius plotted against the distance from the cell soma in the contralateral (left) and ipsilateral (right) CA1 hippocampal region. Grey line: sham-operated animals. Red line: 3 days post-KA injection (KA). Pink line: 1 month post-KA injection (KA chronic). (E) Number of intersections *per* 2 μm radial steps in the contralateral (left) and ipsilateral (right) DG region. (F) Representative morphologies of microglial cells in Iba-1 immunofluorescence coronal sections in the CA1 hippocampal regions are shown for sham, KA and KA chronic animals; the correspondent reconstruction of the microglial cell is illustrated in the lower part of the panel. Left and right (KA-injected) hippocampus are marked by contralateral and ipsilateral, respectively. Calibration bar = 20 μm

animals compared to sham animals (Figure 5D–E). In chronic KA animals, Sholl analysis confirmed microglia morphological changes in the KA-injected ipsilateral hippocampi, whereas values similar to sham condition were found in the contralateral hippocampus (Figure 5D–E). As expected, microglial cells had a lower number of processes (Figure 6A I and B I), total length (Figure 6 A II and B II) and average intersections (Figure 6 A III and B III) at 3 days post-KA in the ipsilateral CA1 and DG in comparison to sham-animals (see also Figure 5F). A similar profile was obtained in the contralateral hippocampi 3-days post KA (Figure 6A I–III and B I–II), except for the DG number of intersections (Figure 6 B III). Interestingly, while in the ipsilateral hippocampus these changes were maintained over time (except average intersections in CA1 - compare the KA chronic groups with the matched sham-groups; in Figure 6A I and II and B I–III), in the contralateral hippocampus of KA chronic animals, all parameters were similar to the respective sham-animals (Figure 6A I–III and B I–III). These experiments show a transient and possibly reversible glial activation pattern, coupled with no apparent cell loss in the hippocampi, contralateral to the KA injection.

We complemented the morphological analysis with the study of gene expression (through mRNA relative expression) in CA1 and DG using quantitative real-time PCR (Figure 7). First, we measured mRNA expression of pro-inflammatory genes, IL1- β and COX-2 (Figure 7A,B, respectively). In line with the densitometry analysis, we observed a higher expression of both genes in the ipsilateral CA1, 3 days post-FncSE with respect to their sham-operated animals; expression was also higher in DG, with statistical significance only for COX-2 (Figure 7B). At one-month post-KA injection, these genes were no longer upregulated. In the contralateral hippocampus, the expression of the aforementioned genes was similar in all groups (Figure 7A,B). Stress-induced gene HO-1 and activity-dependent c-Fos expression were upregulated in the ipsilateral side 3 days post-KA injection compared to sham in CA1 and DG (Figure 7C,D). mRNA expression did not change in the KA chronic group in the ipsilateral side and in all contralateral side groups compared to the respective sham-operated groups (Figure 7C,D). AQP4 expression was higher than in sham animals in the ipsilateral DG at 3 days post-KA injection, but not in KA chronic animals (Figure 7E). Interestingly, higher expression of AQP4 in CA1 and

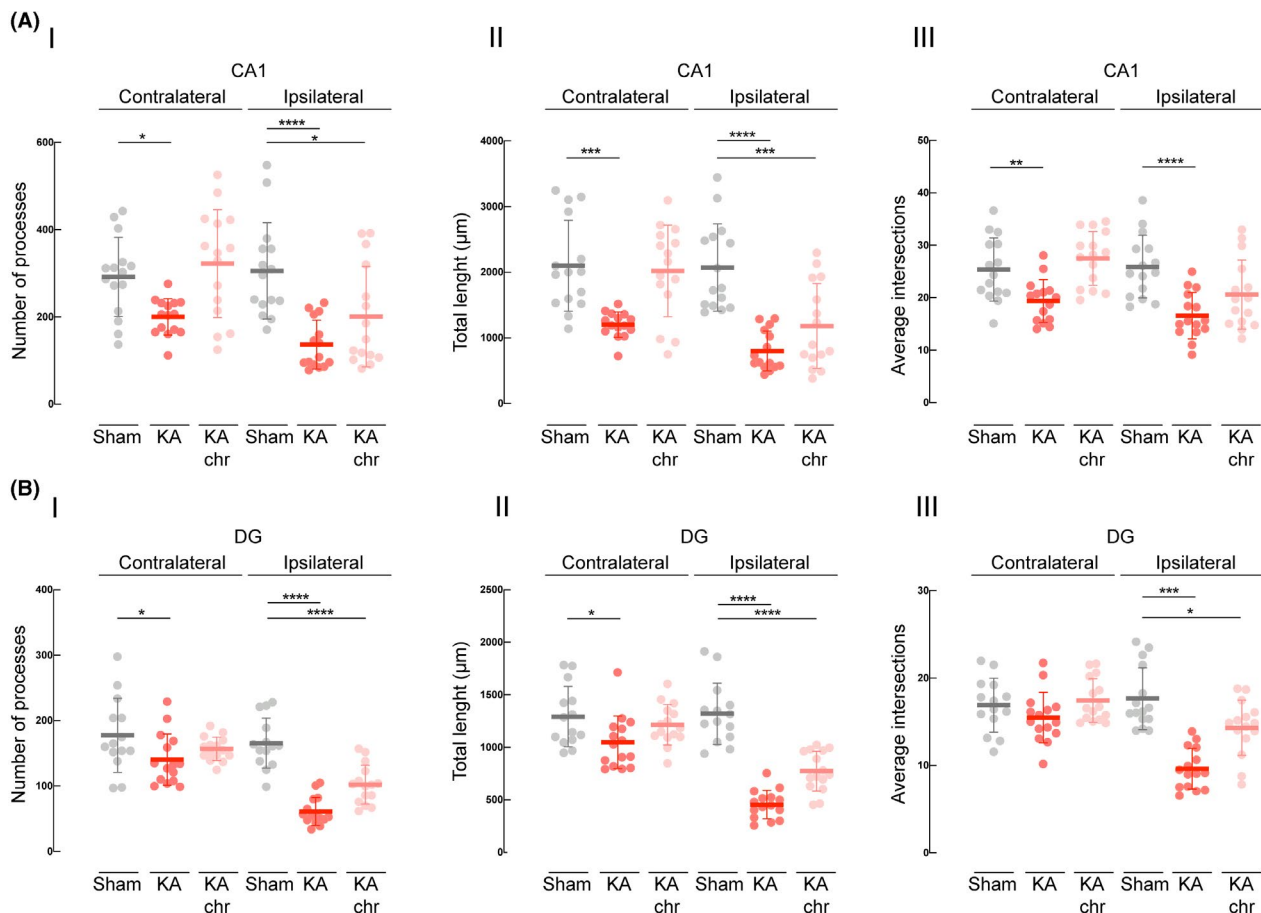


FIGURE 6 Comparative analysis of microglial three dimensional morphology based on Sholl analysis. Grey plots: sham-operated animals. Red plots: 3 days post-KA injection guinea pigs (KA). Pink plots: 1 month post-KA injection animals (KA chronic). (A) Number of processes per 2 μm radius (A I), total length (A II) and average number of intersections (A III) of microglia cells in CA1 hippocampal formation from sham ($n = 15$ cells), KA ($n = 15$ cells) and KA chronic ($n = 15$ cells) guinea pigs (3 cells per animal). ('): $p < 0.05$; (**): $p < 0.01$; (***): $p < 0.001$; (****): $p < 0.0001$ (ANOVA). (B) Number of processes per 2 μm radius (B I), total length (B II) and average number of intersections (B III) of microglia cells in DG from sham ($n = 15$ cells), KA ($n = 15$ cells) and KA chronic ($n = 15$ cells) animals (3 cells per animal). ('): $p < 0.05$; (**): $p < 0.001$; (****): $p < 0.0001$ (ANOVA)

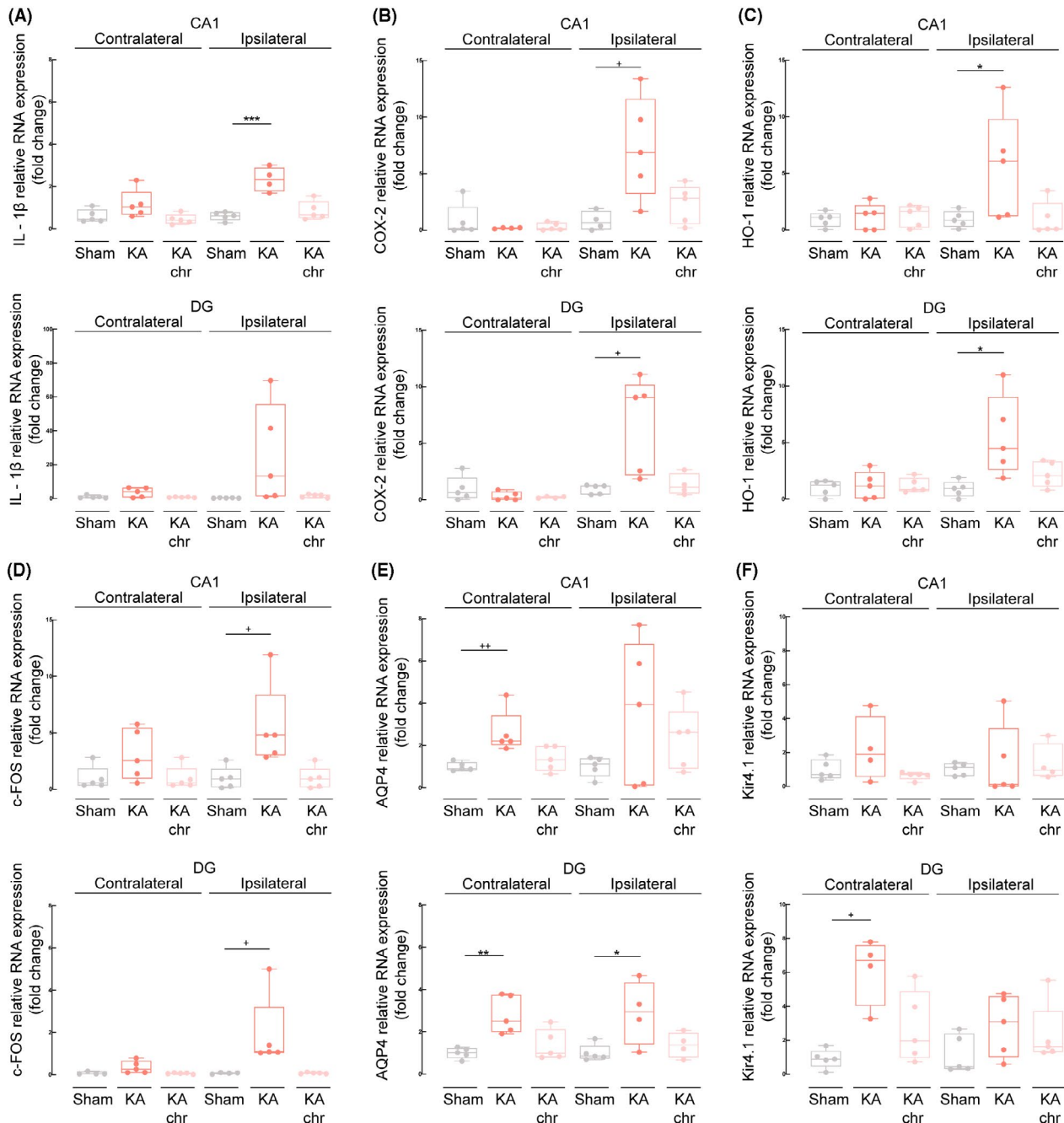


FIGURE 7 Quantitative real-time PCR gene expression analysis of IL-1 β , COX-2, HO-1, c-Fos, AQP4 and Kir4.1 genes. Grey plots: sham-operated animals. Red plots: 3 days post-KA injection guinea pigs (KA). Pink plots: 1 month post-KA injection animals (KA chronic). Average relative mRNA expression (fold change) in the hippocampal CA1 and DG subregions ipsi- and contralateral to KA injection are represented. The mean value of five animals for each of the three groups is reported, unless indicated. All values were normalised to housekeeping genes (Actin and GADPH) as well as to their respective sham-operated animal groups. (A) IL-1 β RNA expression obtained from sham, KA and KA chronic guinea pigs in CA1 (upper graphic) and DG (lower graphic). (***): $p < 0.001$ (ANOVA). (B) COX-2 mRNA expression levels obtained from the same areas of sham ($n = 4-5$), KA and KA chronic ($n = 4-5$) guinea pigs in CA1 (upper graphic) and DG (lower graphic). (†): $p < 0.05$ (Mann-Whitney U test). (C) HO-1 RNA expression levels obtained from the same areas of sham, KA and KA chronic guinea pigs in CA1 (upper graphic) and DG (lower graphic). (†): $p < 0.05$ (ANOVA). (D) c-FOS mRNA expression levels obtained from the same areas of sham, KA and KA chronic guinea pigs in CA1 (upper graphic) and DG (lower graphic). (†): $p < 0.05$ (Mann-Whitney U test). (E) AQP4 mRNA expression levels obtained from the same areas of sham, KA and KA chronic ($n = 4-5$) guinea pigs in CA1 (upper graphic) and DG (lower graphic). (††): $p < 0.01$ (Mann-Whitney U test); (†): $p < 0.05$; (**): $p < 0.01$ (ANOVA). (F) Kir4.1 mRNA expression levels obtained from the same areas of sham, KA and KA chronic ($n = 4-5$) guinea pigs in CA1 (upper graphic) and DG (lower graphic). (†): $p < 0.05$ (Mann-Whitney U test)

DG and Kir4.1 in DG was observed in the contralateral hippocampus as compared to the sham animals (Figure 7E,F), suggesting a seizure activity-mediated upregulation of both genes selectively expressed in astrocytes [39]. These acute changes reverted to sham values in KA chronic animals (Figure 7E,F).

DISCUSSION

The present study analyses a model of FncSE that mimics one of the most frequent and often unrecognised types of human SE. Our results uphold the concept that focal seizures recorded during the course of FncSE have no detrimental effect on the brain unless they are paired with the local excitotoxic effect of KA. Most animal studies that use localised intracerebral KA injection report focal secondarily generalised seizures [20, 21, 40]. The presence of prominent convulsive generalised seizures in these studies is a major confounder for the evaluation of tissue pathology, since convulsive seizures have been demonstrated to promote brain damage via complex generalised and systemic pathogenic mechanisms (for reviews, see [1, 2]).

Our protocol induced a primary epileptogenic area in the hippocampus injected with the KA; within a minute epileptiform activity propagated to the contralateral hippocampus. In this remote secondary region, seizure activity during FncSE was not associated with any underlying damaging event. For the data to be as coherent as possible, all animals included in this study developed a FncSE with focal non-convulsive seizures entraining both hippocampi; focal seizures could secondarily evolve in diffusely propagated epileptiform discharges that correlated with a generated convulsive behaviour (see also [32, 34]). With the exception of 4 animals that presented 10 to 15 secondarily seizures during FncSE, the number of brief (<30 s) convulsive seizures in our experimental group was minimal (1–3 *per* animal, as illustrated in Figure 1F).

In our model the treatment with DZP reduced both the number of seizures during FncSE and FncSE duration itself; these findings correlated with a much-reduced extension of brain damage in the hippocampus ipsilateral to KA injection, as demonstrated by the density of NeuN, MAP2, GFAP, IgG and FJ staining. Even though a direct effect of DZP in reducing the time spent in seizures should also be considered, the less intense cell loss and gliosis observed in DZP-treated animals strongly suggest that the KA-induced damage is partially due to the direct excitotoxic action of KA at the injection site. The larger and more intense distribution of damage markers in the KA-injected hippocampus in the absence of DZP supports the concept that seizure discharges during FncSE are able to exacerbate the KA-induced hippocampal damage. These findings are in line with other studies on focal secondarily generalised seizures induced by local intracerebral KA injections that reported reduced local brain damage at the site of injection when DZP was administered after SE [20, 41, 42]. Our study is the first, to our knowledge, to demonstrate that DZP treatment dramatically reduces focal non-convulsive seizures during FncSE; these changes correlate with reduced damage at the KA injection site.

We analysed neuronal loss by both NeuN and FJ staining that label irreversibly damaged neurons [43] and by MAP2 immunostaining that has been shown to concentrate in neuronal somata during reversible neuronal suffering [44]. Our results showed a consistent and recurrent cell loss and neuronal stress in the ipsilateral hippocampus in KA acute and chronic animals, with no correspondent neuronal loss in the contralateral hippocampus. The FJ results revealed ipsilateral cell loss in the 3 days KA group, with no positive cells observed in the KA chronic group, suggesting that the bulk of apoptotic neurons were produced early after FncSE. Similar findings were published by our group in the same animal model using TUNEL assay that specifically targets DNA-fragmented neurons [32]. Notably, FJ⁺ were not observed in remote brain regions (contralateral hippocampus), where focal seizures during FncSE were also generated. These data are in line with the finding that seizures, after an initial epileptogenic insult, do not lead to progressive cell loss [45]. Moreover, a lack of clear association between the number of lifetime seizures and the severity of neuronal loss in the hilus was shown in a long follow-up study extended 8 months after SE [46, 47]. Similar conclusions were also reported in post-surgical tissue obtained from patients with focal epilepsy submitted to surgery [48]. Nevertheless, there are also several animal studies showing clear progressive neuronal loss produced by seizures not only in the local site of KA injection, but also in remote regions [20, 21, 49]. This discrepancy might be due to the use of protocols that induce a convulsive SE condition rather than a FncSE. In models of proper FncSE developed in different animal species, indeed, remote damage in the hippocampus contralateral to KA injection was never explicitly reported [18, 19, 22–24, 50]. We cannot exclude that stronger and more intense seizure activity could induce secondary damage in remote regions, even though in our experiments, no difference in the extent of damage in both ipsi- and contralateral hippocampi was found in those animals that experienced secondary convulsive seizures during FncSE compared to those with focal seizure only.

The possibility that immunohistochemical changes were not sensitive enough to detect minor changes in regions remote to FncSE was considered and analysed by evaluating gene expression levels in acute and chronic post-SE animals. These experiments revealed that genes associated with inflammatory response (IL1- β and COX-2), brain activity (*c-FOS*) and oxidative stress (HO-1) were upregulated exclusively in the KA-ipsilateral hippocampus early during the acute phase, whereas only genes linked to glial function (AQP4 and Kir4.1) were upregulated 3 days post-KA (but not after 1 month) in the contralateral hippocampus. Glial cells have a plethora of multitasking housekeeping functions such as sensing and responding to alterations in energy supply, neuronal activity, extracellular ion concentrations, osmolarity and many other signals. Their dysfunction has been associated with epilepsy mainly through hyperexcitability and inflammatory-related processes (for extensive reviews see [51, 52]). As observed in other FncSE studies [18, 22, 23, 32], astro- and micro-gliosis in the injected hippocampus was also confirmed in our model. Here, astro- and microgliosis, BBB disruption and

upregulation of inflammatory genes IL1- β and COX-2, as well as stress-related genes c-FOS and HO-1 were evident and persisted 1 month after FncSE in some areas. In contrast, a mild astrocytic and microglial activation was detected in the contralateral hippocampus only at 3 days post-KA with GFAP densitometry analysis and Iba-1 morphological reconstructions. As mentioned above, gliosis was coupled with upregulation of specific astrocytic genes AQP4 and Kir4.1 without overexpression of pro-inflammatory, activity-related or oxidative stress-related genes. Furthermore, 1 month post-KA injection, these alterations returned to basal expression levels comparable to sham-operated animals. A short-lived contralateral microgliosis was also reported, with a significant reduction of microglia complexity, number of processes and total length in CA1 and DG in the acute phase, but not in chronic animals. Overall, these results point towards a possible transient effect mediated by seizure activity on glial cells. Our data do not specifically show, however, if the same cells reverted to their inactivated state or if only the resting/inactivated glial cells remained 1 month after FncSE. Interestingly, these transient effects correlated with the absence of contralateral neuronal loss or BBB leakage. These findings suggest a possible early protective role promoted by glial cells in the hippocampus contralateral to KA injection; the astrocyte-specific expression of AQP4 and Kir4.1 might enhance neuronal potassium clearing during seizure activity. Since both extracellular K⁺ concentration and osmolarity have been shown to dramatically modulate neural excitability [53–56], it is plausible to speculate that astrocytes increase AQP4 and Kir4.1 gene expression as a first line of defence to counter-balance the potential nefarious effect of seizure activity, hence reducing the hyperexcitability through the glial-network. It is unclear however if this compensatory gene upregulation is accompanied by a translation into functional proteins, and further studies are required to address this issue. Nevertheless, studies have shown that a dysfunction of astroglial Kir4.1 channels underlies impaired K⁺ buffering and contributes to hyperexcitability in epileptic tissue [56]. Moreover AQP4^{-/-} mice have remarkably slowed K⁺ reuptake in seizure models and were associated with increased seizure duration, supporting the hypothesis that AQP4 and Kir4.1 can act together in K⁺ and H₂O regulation [54]. In line with our findings, an acute reactive astrogliosis and microgliosis that decreased over time in the contralateral hippocampus but remained altered in the KA-injected hippocampus was reported in an unilateral intrahippocampal KA mouse model [24]. This study reported a delayed upregulation in the contralateral hippocampus of SOCS3, which acts by limiting IL-6 mediated processes, possibly indicating an attempt to limit the intensity/duration of neuroinflammatory signals during the early phase of epileptogenesis. The authors hypothesised that the SOCS3 mRNA increase could be involved in neuronal survival and/or induction of homeostatic mechanisms against neurodegeneration by limiting cytokine signalling in the contralateral hippocampus.

In conclusion, in our FncSE model brain tissue damage is aggravated by seizure activity when it occurs in combination with

the excitotoxic effect of KA. The secondary spread of seizure activity to the contralateral hippocampus transiently activated glial cells, as a potential defence mechanism that prevented remote seizure-associated damage. These results might only hold true for this particular dosage of KA and/or for the specific seizure-FncSE pattern generated in this animal model. Even though the experimental findings here reported cannot directly be translated into clinical conclusions, our study recommends the use of anti-seizure treatment in patients suffering from FncSE to prevent further localised seizure-mediated damage in addition to the injury determined by the primary *noxa*. When combined with a coexisting insult, seizures can work synergistically to further exacerbate the damage done by the underlying FncSE cause. However, if seizure activity spreads to regions away from the boundaries of the primary injury constraint, a detrimental action caused by seizures *per se* is not likely to occur.

ACKNOWLEDGMENTS

None of the authors has any conflict of interest to disclose. We confirm that we have read the Journal's position on issues involved in ethical publication and affirm that this report is consistent with those guidelines. This work was supported by: the European Union's Horizon 2020 Research and Innovation Programme under the Marie Skłodowska-Curie grant agreement no. 722053 (EU-GliaPhD; DVV, TSZ, EA, MC) and agreement no. 765966 (EpiSyStem; MFP, GT), the Italian Health Ministry (Ricerca Corrente 2018-2020) and the EPICARE project of the Associazione Paolo Zorzi per le Neuroscienze.

AUTHOR CONTRIBUTIONS

DVV, MdC, EA and EV contributed to conception and design of the study. DVV, TZ, AC, MFP, GT and VG contributed to acquisition and analysis of data. DVV and MdC contributed to drafting a significant portion of the manuscript or figures.

Our experimental protocol has been ethically reviewed and approved by the Animal Welfare Office of the Italian Health Ministry (Authorization n. 36/2016-PR), in accordance with the European Committee Council Directive (2010/63/EU) and with the 3Rs principle.

PEER REVIEW

The peer review history for this article is available at <https://publons.com/publon/10.1111/nan.12693>.

DATA AVAILABILITY STATEMENT

The data that support the findings of this study are available from the corresponding author upon reasonable request.

ORCID

Diogo Vila Verde  <https://orcid.org/0000-0003-3084-6552>

Marlene F. Pereira  <https://orcid.org/0000-0002-8890-2994>

Erwin van Vliet  <https://orcid.org/0000-0001-5747-3202>

Marco de Curtis  <https://orcid.org/0000-0001-7443-6737>

REFERENCES

1. Wasterlain CG, Fujikawa DG, Penix LR, Sankar R. Pathophysiological mechanisms of brain damage from status epilepticus. *Epilepsia*. 1993;34:37-53.
2. Shorvon S. Does convulsive status epilepticus (SE) result in cerebral damage or affect the course of epilepsy - the epidemiological and clinical evidence? *Prog Brain Res*. 2002;135:85-93.
3. Young GB, Claassen J. Nonconvulsive status epilepticus and brain damage: Further evidence, more questions. *Neurology*. 2010;75:760-770.
4. Claassen J, Mayer SA, Kowalski RG, Emerson RG, Hirsch LJ. Detection of electrographic seizures with continuous EEG monitoring in critically ill patients. *Neurology*. 2004;62:1743-1748.
5. Trinka E, Cock H, Hesdorffer D, et al. A definition and classification of status epilepticus - report of the ILAE Task Force on Classification of Status Epilepticus. *Epilepsia*. 2015;56:1515-1523.
6. Rabinowicz AL, Correale JD, Bracht KA, Smith TD, DeGiorgio CM. Neuron-specific enolase is increased after nonconvulsive status epilepticus. *Epilepsia*. 1995;36:475-479.
7. Cockerell OC, Walker MC, Sander JWAS, Shorvon SD. Complex partial status epilepticus: a recurrent problem. *J Neurol Neurosurg Psychiatry*. 1994;57:835-837.
8. Guberman A, Cantu-Reyna G, Stuss D, Broughton R. Nonconvulsive generalized status epilepticus: clinical features, neuropsychological testing, and long-term follow-up. *Neurology*. 1986;36:1284-1291.
9. Kaplan PW. No, some types of nonconvulsive status epilepticus cause little permanent neurologic sequelae (or: « The cure may be worse than the disease »). *Neurophysiol Clin*. 2000;30:377-382.
10. Gutierrez C, Chen M, Feng L, Tummala S. Non-convulsive seizures in the encephalopathic critically ill cancer patient does not necessarily portend a poor prognosis. *J Intensive Care*. 2019;7:1-9.
11. Sperk G. Kainic acid seizures in the rat. *Prog Neurobiol*. 1994;42:1-32.
12. Curia G, Longo D, Biagini G, Jones RSG, Avoli M. The pilocarpine model of temporal lobe epilepsy. *J Neurosci Methods*. 2008;172:143-157.
13. Lévesque M, Avoli M. The kainic acid model of temporal lobe epilepsy. *Neurosci Biobehav Rev*. 2013;37:2887-2899.
14. Sloviter RS. Hippocampal epileptogenesis in animal models of mesial temporal lobe epilepsy with hippocampal sclerosis: the importance of the "latent period" and other concepts. *Epilepsia*. 2008;49:85-92.
15. Henshall DC. Poststatus epilepticus models: focal kainic acid. In: Pitkänen A, Galanopoulou AS, Buckmaster PS, Moshé SL, eds. *Models of Seizures and Epilepsy*. 2nd ed. Cambridge, MA, USA: Academic Press. 2017:611-624.
16. Riban V, Bouillere V, Pham-Lê BT, Fritschy JM, Marescaux C, Depaulis A. Evolution of hippocampal epileptic activity during the development of hippocampal sclerosis in a mouse model of temporal lobe epilepsy. *Neuroscience*. 2002;112:101-111.
17. Arabadzisz D, Antal K, Parpan F, Emri Z, Fritschy JM. Epileptogenesis and chronic seizures in a mouse model of temporal lobe epilepsy are associated with distinct EEG patterns and selective neurochemical alterations in the contralateral hippocampus. *Exp Neurol*. 2005;194:76-90.
18. Bouillere V, Ridoux V, Depaulis A, et al. Recurrent seizures and hippocampal sclerosis following intrahippocampal kainate injection in adult mice: electroencephalography, histopathology and synaptic reorganization similar to mesial temporal lobe epilepsy. *Neuroscience*. 1999;89:717-729.
19. Tanaka T, Tanaka S, Fujita T, et al. Experimental complex partial seizures induced by a microinjection of kainic acid into limbic structures. *Prog Neurobiol*. 1992;38:317-334.
20. Ben-Ari Y, Tremblay E, Ottersen OP, Meldrum BS. The role of epileptic activity in hippocampal and "remote" cerebral lesions induced by kainic acid. *Brain Res*. 1980;5:515-518.
21. Schwob JE, Fuller T, Price JL, Olney JW. Widespread patterns of neuronal damage following systemic or intracerebral injections of kainic acid: a histological study. *Neuroscience*. 1980;5:991-1014.
22. Mouri G, Jimenez-Mateos E, Engel T, et al. Unilateral hippocampal CA3-predominant damage and short latency epileptogenesis after intra-amygdala microinjection of kainic acid in mice. *Brain Res*. 2008;1213:140-151.
23. Bedner P, Dupper A, Hüttmann K, et al. Astrocyte uncoupling as a cause of human temporal lobe epilepsy. *Brain*. 2015;138:1208-1222.
24. Pernet F, Heinrich C, Barbier L, et al. Inflammatory changes during epileptogenesis and spontaneous seizures in a mouse model of mesiotemporal lobe epilepsy. *Epilepsia*. 2011;52:2315-2325.
25. Ben-Ari Y. Limbic seizure and brain damage produced by kainic acid: mechanisms and relevance to human temporal lobe epilepsy. *Neuroscience*. 1985;14:375-403.
26. Rattka M, Brandt C, Löscher W. The intrahippocampal kainate model of temporal lobe epilepsy revisited: epileptogenesis, behavioral and cognitive alterations, pharmacological response, and hippocampal damage in epileptic rats. *Epilepsy Res*. 2013;103:135-152.
27. Sloviter RS. "Epileptic" brain damage in rats induced by sustained electrical stimulation of the perforant path. I. Acute electrophysiological and light microscopic studies. *Brain Res Bull*. 1983;10:675-697.
28. Lothman EW, Bertram EH, Bekenstein JW, Perlin JB. Self-sustaining limbic status epilepticus induced by "continuous" hippocampal stimulation: electrographic and behavioral characteristics. *Epilepsy Res*. 1989;3:107-119.
29. Mazarati AM, Wasterlain CG, Sankar R, Shin D. Self-sustaining status epilepticus after brief electrical stimulation of the perforant path. *Brain Res*. 1998;801:251-253.
30. Gorter JA, Van Vliet EA, Lopes da Silva FH, Isom LL, Aronica E. Sodium channel β 1-subunit expression is increased in reactive astrocytes in a rat model for mesial temporal lobe epilepsy. *Eur J Neurosci*. 2002;16:360-364.
31. Avdic U, Ahl M, Chugh D, et al. Nonconvulsive status epilepticus in rats leads to brain pathology. *Epilepsia*. 2018;59:945-958.
32. Noè F, Cattalini A, Vila Verde D, et al. Epileptiform activity contralateral to unilateral hippocampal sclerosis does not cause the expression of brain damage markers. *Epilepsia*. 2019;1-16.
33. Carriero G, Arcieri S, Cattalini A, Corsi L, Gnatkovsky V, De Curtis M. A guinea pig model of mesial temporal lobe epilepsy following nonconvulsive status epilepticus induced by unilateral intrahippocampal injection of kainic acid. *Epilepsia*. 2012;53:1917-1927.
34. Arcieri S, Velotti R, Noè F, et al. Variable electrobehavioral patterns during focal nonconvulsive status epilepticus induced by unilateral intrahippocampal injection of kainic acid. *Epilepsia*. 2014;55:1978-1985.
35. Tavares G, Martins M, Correia JS, et al. Employing an open-source tool to assess astrocyte tridimensional structure. *Brain Struct Funct*. 2017;222:1989-1999.
36. van Scheppingen J, Iyer AM, Prabowo AS, et al. Expression of microRNAs miR21, miR146a, and miR155 in tuberous sclerosis complex cortical tubers and their regulation in human astrocytes and SEGAs-derived cell cultures. *Glia*. 2016;64:1066-1082.
37. Racine RJ. Modification of seizure activity by electrical stimulation: II. Motor seizure. *Electroencephalogr Clin Neurophysiol*. 1972;32:281-294.
38. Noé FM, Bellistri E, Colciaghi F, et al. Kainic acid-induced albumin leak across the blood-brain barrier facilitates epileptiform hyperexcitability in limbic regions. *Epilepsia*. 2016;57:967-976.

39. Song Y, Gunnarson E. Potassium dependent regulation of astrocyte water permeability is mediated by camp signaling. *PLoS One*. 2012;7:e34936.
40. Mathern GW, Cifuentes F, Leite JP, Pretorius JK, Babb TL. Hippocampal EEG excitability and chronic spontaneous seizures are associated with aberrant synaptic reorganization in the rat intra-hippocampal kainate model. *Electroencephalogr Clin Neurophysiol*. 1993;87:326-339.
41. Pollard H, Charriaut-Marlangue C, Cantagrel S, et al. Kainate-induced apoptotic cell death in hippocampal neurons. *Neuroscience*. 1994;63:7-18.
42. Pitkänen A, Kharatishvili I, Narkilahti S, Lukasiuk K, Nissinen J. Administration of diazepam during status epilepticus reduces development and severity of epilepsy in rat. *Epilepsy Res*. 2005;63:27-42.
43. Schmued LC, Albertson C, Slikker W. Fluoro-Jade: a novel fluorochrome for the sensitive and reliable histochemical localization of neuronal degeneration. *Brain Res*. 1997;751:37-46.
44. Johnson GVW, Jope RS. The role of microtubule-associated protein 2 (MAP-2) in neuronal growth, plasticity, and degeneration. *J Neurosci Res*. 1992;33:505-512.
45. Bertram EH, Lothman EW, Lenn NJ. The hippocampus in experimental chronic epilepsy: a morphometric analysis. *Ann Neurol*. 1990;27:43-48.
46. Nairismägi J, Gröhn OHJ, Kettunen MI, Nissinen J, Kauppinen RA, Pitkänen A. Progression of brain damage after status epilepticus and its association with epileptogenesis: a quantitative MRI study in a rat model of temporal lobe epilepsy. *Epilepsia*. 2004;45:1024-1034.
47. Pitkänen A, Nissinen J, Nairismägi J, et al. Progression of neuronal damage after status epilepticus and during spontaneous seizures in a rat model of temporal lobe epilepsy. *Prog Brain Res*. 2002;135:67-83.
48. Rossini L, Garbelli R, Gnatkovsky V, et al. Seizure activity *per se* does not induce tissue damage markers in human neocortical focal epilepsy. *Ann Neurol*. 2017;82:331-341.
49. Cavazos JE, Das I, Sutula TP. Neuronal loss induced in limbic pathways by kindling: evidence for induction of hippocampal sclerosis by repeated brief seizures. *J Neurosci*. 1994;14:3106-3121.
50. French ED, Aldinio C, Schwarcz R. Intra-hippocampal kainic acid, seizures and local neuronal degeneration: relationships assessed in unanesthetized rats. *Neuroscience*. 1982;7:2525-2536.
51. Vezzani A, Granata T. Brain inflammation in epilepsy: experimental and clinical evidence. *Epilepsia*. 2005;46:1724-1743.
52. Devinsky O, Vezzani A, O'Brien TJ, et al. Epilepsy. *Nat Rev Dis Prim*. 2018;4:18-24.
53. Binder DK, Steinhäuser C. Functional changes in astroglial cells in epilepsy. *Glia*. 2006;54:358-368.
54. Binder DK, Yao X, Zador Z, Sick TJ, Verkman AS, Manley GT. Increased seizure duration and slowed potassium kinetics in mice lacking aquaporin-4 water channels. *Glia*. 2006;53:631-636.
55. Seifert G, Steinhäuser C. Neuron-astrocyte signaling and epilepsy. *Exp Neurol*. 2013;244:4-10.
56. Steinhäuser C, Seifert G. Glial membrane channels and receptors in epilepsy: Impact for generation and spread of seizure activity. *Eur J Pharmacol*. 2002;447:227-237.

SUPPORTING INFORMATION

Additional supporting information may be found online in the Supporting Information section.

How to cite this article: Vila Verde D, Zimmer T, Cattalini A, et al. Seizure activity and brain damage in a model of focal non-convulsive status epilepticus. *Neuropathol Appl Neurobiol*. 2021;47:679–693. <https://doi.org/10.1111/nan.12693>